process contributes negligibly to the absorption in comparison with the (a) process. Hence, we are unable to draw rigid conclusions regarding the applicability of the rule to indirect transitions without a detailed knowledge of the band structure of a specific solid.

Recently Balkanski and Waldron[28] have studied the CdS and ZnS systems experimentally. Their absorption curves for CdS are in agreement with the selection rule in the fundamental region. The absorption for long wavelengths, which is dependent upon impurity content, exhibits a violation of the rule. As the authors have noted, one cannot expect band-to-band selection rules to apply at these wavelengths. For this reason, since their data for ZnS do not extend into the fundamental region, their results, which happen to agree with the rule, cannot be interpreted within the framework of the present analysis without additional assumptions. As mentioned earlier, the rule is verified for ZnS by the work of Piper *et al.*[14] and Keller and Pettit[22] whose measurements extend well into the region of fundamental absorption.

[28] M. Balkanski and R. D. Waldron, Phys. Rev. **112**, 123 (1958).

ACKNOWLEDGMENTS

I wish to thank Dr. R. E. Behringer and Dr. G. Lasher for stimulating discussions and Dr. J. Slonczewski for helpful comments regarding the manuscript.

PHYSICAL REVIEW VOLUME 114, NUMBER 6 JUNE 15, 1959

Temperature Dependence of the Electrical Properties of Bismuth-Antimony Alloys*†

A. L. JAIN
Department of Physics and Institute for the Study of Metals, University of Chicago, Chicago, Illinois
(Received January 22, 1959)

The electrical resistivity ρ and Hall effect R of zone-levelled single crystals of Bi-Sb alloys have been measured in the temperature range from 4.2°K to 300°K. $\mathrm{Log}(\rho/\rho_{300})$ *vs* $1/T$ curves suggest thermal activation of carriers in the concentration range from 5% to 40% Sb in the temperature range from 25°K to 100°K; approximate activation energies have been inferred from their slopes. The activation energy appears to have a maximum at a concentration near 12%. Some anomalies have been observed in the behavior of ρ and R on both sides of this concentration at low temperatures. Lattice parameters for these alloys have also been measured for the entire range of solid solubility. Both a maximum and minimum in the c-axis lattice parameter *vs* concentration occur near the concentration at which anomalies appear in transport properties. These phenomena are discussed in terms of a simple band model proposed by Blount and Cohen.

I. INTRODUCTION

RHOMBOHEDRAL bismuth is a semimetal with a carrier concentration of about $10^{18}/\mathrm{cm}^3$. Some information concerning the band structure has been obtained from measurements of de Haas-van Alphen effect,[1] cyclotron resonance,[2] galvanomagnetic[3] effects, and elastoresistance.[4] These effects have been interpreted in terms of the conduction band overlapping upon the valence band by 0.0184 ev. This overlap gives rise to the small number of electrons in the conduction and an equal number of holes in the valence band. The experimental results are all consistent with a Fermi surface composed of a set of 3 ellipsoids for electrons and an ellipsoid of revolution around the trigonal axis for holes. The three ellipsoids can be transformed into one another by 120° rotations around the trigonal axis. Combining the de Haas-van Alphen effect data with their specific heat data at low temperatures, Kalinkina and Strekov[5] have determined the mean effective mass of holes to be $m_h^* \cong 2.5 m_0$ which is very large compared to that of electrons $m_e^* \cong 0.05 m_0$ given by Shoenberg.[1]

Further information about the band structure in bismuth can be obtained from the electrical and magnetic properties of its alloys. It was realized by Jones[6] that alloying bismuth with small amounts of elements with different valence might permit the study of either an electron band or a hole band separately. Thompson[7] has indeed carried out above 15°K extensive measurements of the electrical properties of bismuth alloys containing Pb, Sn, Se, Te, as well as less extensive studies of other alloys. The group IV elements Pb and Sn act as acceptors much as do group III elements in the silicon-germanium type of semiconductor. Similarly,

* Submitted as a thesis in partial fulfillment of the requirements for the degree of Doctor of Philosophy at the University of Chicago.

† The work was supported in part by a grant from the National Science Foundation to the University of Chicago for research on the solid-state properties of bismuth, antimony, and arsenic.

[1] J. S. Dhillon and D. Shoenberg, Trans. Roy. Soc. (London) **A248**, 1 (1955).

[2] J. E. Aubrey and R. G. Chambers, J. Phys. Chem. Solids **3**, 128 (1957).

[3] B. Abeles and S. Meiboom, Phys. Rev. **101**, 544 (1956).

[4] R. W. Keyes, Phys. Rev. **104**, 665 (1956).

[5] I. N. Kalinkina and P. G. Strekov, J. Exptl. Theoret. Phys. U.S.S.R. **34**, 616 (1958) [translation: JETP **7**, 426 (1958)].

[6] H. Jones, Proc. Roy. Soc. (London) **A147**, 396 (1934).

[7] N. Thompson, Proc. Roy. Soc. (London) **A155**, 111 (1936); **A164**, 24 (1938).

group VI elements act as donors. Abeles and Meiboom[3] have effectively exploited this concept in their experimental study of galvanomagnetic effects and Heine[8] has analyzed the measurements of Shoenberg and Uddin[9] on magnetic susceptibility of Bi-Sn, Bi-Pb, and Bi-Te alloys at low temperatures on the same basis. However, according to Blount and Cohen,[10] the addition of donors and acceptors can be expected to modify the band structure of bismuth as well as change the carrier concentration. The differences in the properties of Bi-Sn and Bi-Pb alloys[7,9] illustrate the former effect. The addition of group V elements, however, can be expected to modify the band structure without destroying the equality of electron and hole concentration.

Thus, a comparison of the properties of alloys containing group V elements with those containing group IV or VI should help to unravel the two effects. Of the group V elements, Sb is the most promising impurity for study because it is the most similar to Bi and, in addition, forms a complete range of solid solutions. The present investigation was undertaken for three reasons.

Shoenberg and Uddin[9] suggest on the basis of de Haas-van Alphen measurements on Bi-Sb alloys that the Fermi energy decreases with addition of Sb. Heine[8] has pointed out that a decreased Fermi energy implies a decreased overlap and that, consequently, Bi-Sb alloys may become semiconducting at concentrations of Sb greater than 4%. The early work of Smith[11] is consistent with this observation.[10] Thompson's measurements of the electrical resistance of a 10% Sb alloy do show a resistivity which increases as the temperature decreases to about 50°K. However, below this temperature, the resistance begins to drop in contrast to normal semiconducting behavior.

Because the carrier density is small and varying rapidly with concentration, it is necessary to carry out the measurements at low temperatures on single crystal samples of controlled and homogeneous composition. The earlier experimental work was inadequate in this respect.

This paper reports the results of measurements of the electrical properties of such samples as functions of Sb composition up to 41%. The electrical conductivity along the binary axis and both independent Hall constants were measured between 4.2°K and 300°K. Some data on magnetoresistance were obtained at 4.2°K.

Results of our investigation have been discussed in terms of the model proposed by Blount and Cohen which is illustrated schematically in Fig. 1. According to this scheme the pertinent part of the band structure of pure bismuth [Fig. 1(a)] consists of a pair of light

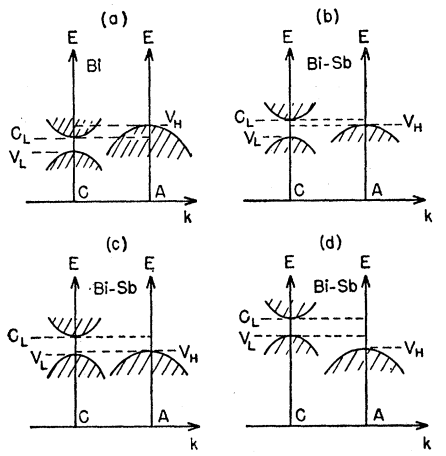

FIG. 1. E *vs* k diagrams for bismuth and bismuth-antimony alloys. C_L and V_L represent the light mass bands, each having six extrema in k-space. V_H is the heavy mass band having two extrema. Case (a): Pure bismuth. V_H overlaps upon C_L. (b): $C_L-V_H<C_L-V_L$ (c): $C_L-V_L=C_L-V_H$ (d): $C_L-V_L<C_L-V_H$.

mass bands at six symmetrically related positions in **k**-space, the upper of which is occupied by electrons and a heavy mass hole band at 2 positions in **k**-space.[12] The effect of antimony is to displace the heavy mass band downward with respect to the light mass band as indicated in Fig. 1 (b), (c), (d). The results of our investigation show that the model is incomplete, especially with regard to its predictions for the low-temperature behavior of the alloys.

Another prediction of the model is that the lattice parameter should depend significantly on antimony concentration. Room temperature measurements of the lattice parameters of the alloys show that they deviate appreciably from Vegard's law at concentrations where electrical properties are changing drastically.

II. EXPERIMENTAL METHODS

Preparation and Analysis of Samples

Bismuth purchased from the Cerro de Pasco Company of label purity 99.998% was processed further by zone melting ten times in a quartz boat in vacuum of about 10^{-6} mm Hg. The zone refining apparatus was similar to one described elsewhere.[13] High purity antimony was obtained from the Ohio Semiconductor Company. A careful spectrographic analysis of samples before and after alloying failed to show any impurities. Limits of impurity content are given in Table I. These figures are estimated from the sensitivity of the spectrographic analysis. Homogeneous alloys were prepared by melting bismuth and anitmony together in two successive stages. Initially a known amount of antimony was

[8] V. Heine, Proc. Phys. Soc. (London) **A69**, 513 (1956).
[9] D. Shoenberg and M. Z. Uddin, Proc. Roy. Soc. (London) **A156**, 687–701 (1936).
[10] E. I. Blount and M. H. Cohen (private communication).
[11] A. W. Smith, Phys. Rev. **32**, 178 (1911).
[12] This doubling of the number of electrons and hole positions comes from inversion symmetry.
[13] W. G. Pfann, in *Solid State Physics*, edited by F. Seitz and D. Turnbull (Academic Press, Inc., New York, 1957), Vol. 4.

TABLE I. Impurity content of zone-refined elements.

Bismuth		Antimony	
Impurity	Wt. (%)	Impurity	Wt. (%)
Pb	0.0003	Te	0.00001
Si	0.00001	Zn	0.00001
Ag	0.00001	Cd	0.00001
Ni	0.00001		
Cu	0.00001		

allowed to dissolve in molten bismuth contained in a 10-in. fused quartz boat. The ingot so obtained was then zone melted several times. The molten zone was adjusted to be about $\frac{3}{4}$ in. in length so that all deviations from a uniform composition remaining after the first melting stage were greatly reduced except in the last zone to freeze. According to Pfann this process of eliminating points of high and low concentration is particularly effective if $|1-k|$ is large, where k is the ratio of concentration of impurity in the solid to that in the liquid at equilibrium. The value of k as deduced from the phase diagram[14] varies from 5 to 8 at low concentration and thus the process appeared quite suitable for obtaining a high degree of homogeneity in Bi-Sb alloys. In order to ensure a uniform mixing in the molten zone and thus to minimize fluctuations in the concentration, inductive heating at 450 kc was used. The boat was pulled in both directions at a constant rate of 2 in./hr. All the melting processes were carried on in vacuum or in a helium atmosphere to avoid any oxidation on the surface which, if present, resulted in a polycrystalline sample. Before use, all the quartz boats were first soaked in hydrofluoric acid for several hours and then rinsed thoroughly with distilled water. This procedure eliminated scratches on the surface of the boats reducing extraneous sources of nucleation. Following this procedure it was possible to get large crystals approximately 8 in. $\times\frac{1}{2}$ in. $\times\frac{1}{2}$ in. Chemical analysis showed these crystals to have a variation of less than 3% of the mean value along a one inch sample cut from the central part of the ingot. The crystallographic directions of the crystal were determined with the help of the principal cleavage plane and a Laue pattern. Since the crystals were highly brittle and easily cleavable, samples were first cut into plates with their surfaces parallel to cleavage plane using a 280 mesh carborundum wheel, or by cleavage, and then reduced to the proper dimensions by grinding with a 600 mesh silicon carbide paper. In order to avoid any size effects, samples of rectangular shape with approximate dimensions $3\times3\times20$ mm were used. Finally, the samples were etched with a solution of 95% hydrochloric acid and 5% nitric acid and annealed for about 24 hours at 250°C.

TABLE II. Errors in chemical analysis.

Antimony concentration atomic %	Maximum relative % of error
1–5%	5.0%
6–10%	1.5%
10–70%	1.0%

[14] M. Hansen, *Aufbau der Zweistofflegierung* (Verlag Julius Springer, Berlin, 1936).

In order to obtain lattice parameters for these alloys, powder specimens, mounted in thin walled capillary tubes, were examined with a North American Phillips 114.6-mm camera using filtered copper K radiation. The composition of alloys was determined by Dr. Bachelder of this Institute by the following procedure. The sample was first dissolved in concentrated sulphuric acid and then sufficient hydrochloric acid was added to give a solution of 10% hydrochloric acid and 10% sulphuric acid. Finally the amount of antimony was determined by titration with approximately 0.03N potassium permanganate. The accuracy of the method was checked by analyzing synthetic samples. The maximum relative percent error is given below for various ranges of concentration in Table II.

Cryostat and the Electrical Equipment

The sample holder consisted of a copper plug held in the middle of a copper can by brass screws as shown schematically in Fig. 2. The lower end of the plug carried a varnished copper bracket against which the sample was mounted vertically in good thermal contact. The upper end of the can had a wide opening filled with activated charcoal to increase the heat capacity. A No. 30 manganin wire wound round the copper can served as a heater resistance to allow rapid increases of temperature. Without any external heat input, the heat capacity of the activated charcoal was sufficient to keep the temperature fairly constant during an observation, the warm up rate being less than 1 degree an hour. The copper can was supported inside the helium cryostat by a long, thin-walled stainless steel tube passed through an O-ring seal so that the sample could be rotated about the vertical axis for the alignment of the crystal's principal axis parallel to the magnetic field. This arrangement also permitted the height of the sample to be adjusted between the pole pieces of the magnet. Below 4.2°K, the temperature was measured by a helium vapor pressure thermometer. In the range from 4.2°K to 300°K, it was measured by a 100-ohm carbon resistance thermometer or a copper-constantan thermocouple which were attached to the copper bracket on which the sample was mounted. The effect of the magnetic field on the calibration of these devices was inappreciable.

For electrical measurements, the arrangement of the current and the potential leads was as shown in Fig. 3. Current leads of copper wire (A.W.G. No. 32) were attached to the ends of the sample using Cerro de Pasco's low melting point solder. The three potential leads were also of copper wire (A.W.G. No. 38). In the

case of low concentration alloys and pure bismuth, it was possible to attach potential leads to the sample by discharging a 100 mfd condenser initially charged to a potential of approximately 60 volts. For high concentrations, a rigid joint could not be made by this method and low melting point solder was used for attaching potential leads to these alloys. For electrical resistivity, a current of 0.1 amp was passed through the sample and the potential difference between leads C and D was measured. For Hall effect measurements, a high resistance of 1000 ohms was introduced between the contacts C and D and the sliding contact F was adjusted so as to give zero potential drop between E and F in the absence of the magnetic field. In this way it was possible to

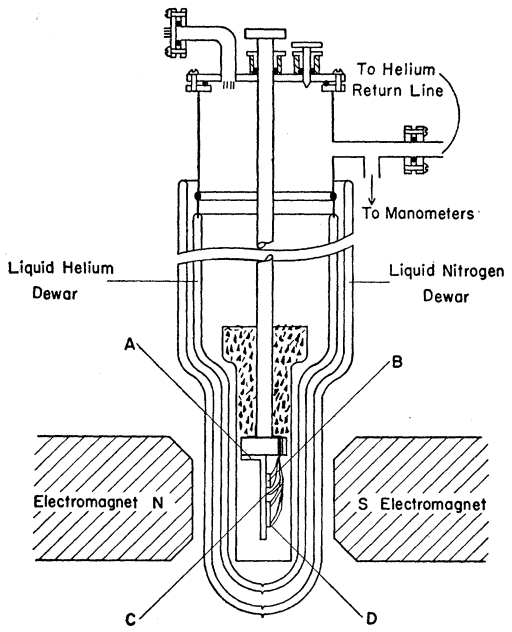

FIG. 2. Schematic diagram of the cryostat and the sample holder: A, copper bracket; B, the carbon resistance thermometer; C, copper-constantan thermocouple; D, sample under investigation.

eliminate spurious misalignment voltages. In order to avoid any thermoelectric effects, the potential drop was always measured for direct and reversed current. The effect of the magnetic field on the thermoelectric voltage was inappreciable over the entire range of concentration and temperature. All the potential differences were measured using a Leeds and Northrup Company's type K2 potentiometer and a Rubicon's galvanometer having a sensitivity of 1.1 μv/mm under critically damped conditions. The current through the sample was determined from the potential drop across a 0.01-ohm standard resistance in series with the sample. The magnetic field was determined by measuring the Hall voltage generated in a germanium crystal at room temperature. This Hall effect gauge was calibrated by means of proton magnetic resonance.

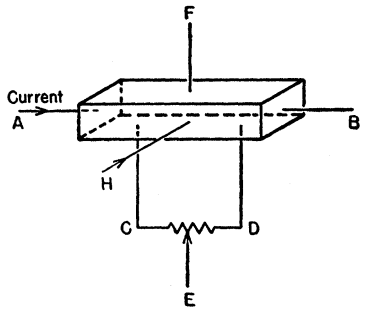

FIG. 3. Arrangement of current and potential leads to the sample for electrical measurements.

Experimental Errors

Electrical quantities were measured with a precision better than 1%. Absolute value of resistivity is accurate to within 10% and the main source of error lies in the determination of the distance between potential leads. Because of slight misorientation ($\pm 2°$) of the crystalline axes relative to the magnetic field, an error of 15% was estimated in Hall coefficient. In the high temperature region, background emf's of the order of 2μv give rise to slightly higher uncertainty in the Hall coefficient.

III. RESULTS

Electrical Resistivity and Hall Effect

The electrical resistivity has been measured for samples of several concentrations in the temperature region from 4.2°K to 300°K. In all these samples, the current flow was along the binary axis of the crystal. Since the error involved in the measurement of the distance between potential leads is significant, the results have been plotted in terms of $\log(\rho/\rho_{300})$ *vs* $1/T$. Figure 4 shows the behavior of the resistivity between

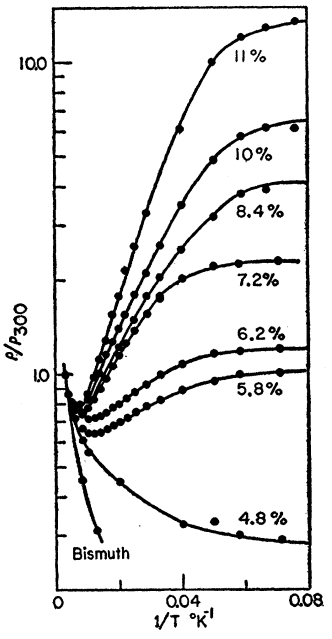

FIG. 4. The ratio of the resistivity to that at 300°K *versus* the reciprocal of the absolute temperature for samples containing 0 to 11% Sb between 20°K to 300°K.

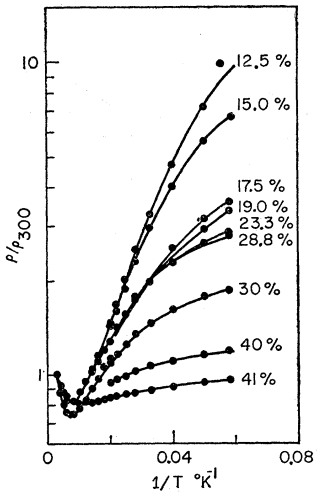

FIG. 5. The ratio of the resistivity to that at 300°K *versus* the reciprocal of the absolute temperature for samples containing 12.5%–41% Sb between 20°K–300°K.

20°K and 300°K for samples containing less than 11.5 atomic percent of antimony. Similar curves are drawn in Fig. 5 for higher concentrations. The measurements indicate a linear dependence of ρ on temperature above 200°K for all the samples. The resistivity decreases monotonically with temperature for concentrations below 5%. We term this behavior as "semimetallic." For concentrations between 5% and 40%, the resistivity starts increasing below 100°K. In the temperature region 30°K–100°K, $\log(\rho/\rho_{300})$ is nearly proportional to $1/T$. However, these alloys are not semiconducting in the usual sense as is shown by the behavior of resistivity data below 25°K presented in Figs. 6 and 7. In this temperature region the resistivity is found to depend only slightly on temperature or traces of impurities, contrary to the behavior observed in a typical semiconductor. Thompson's measurements for a 10% sample do show an increase in resistivity below 200°K down to 50°K, but below 50°K starts decreasing rapidly which is contrary to our results. This discrepancy may arise from inhomogeneity in Thompson's sample.

For samples containing 5% to 11.5% Sb, the temperature dependence of the resistivity between 30°K and 100°K can be described by the expression

$$\rho=\rho_0 \exp(E_g/2kT). \quad (1)$$

For these concentrations, E_g is determined from the slope of $\log(\rho/\rho_{300})$ *vs* $1/T$. For higher concentrations, the behavior of the resistivity is not too well represented by Eq. (1). Therefore the maximum slope has been measured for these alloys and has been assumed to be $E_g/2k$. The variation of E_g with concentration (Fig. 8) shows a maximum at 12%. On Blount and Cohen's model, E_g can be regarded as a measure of the energy gap between the conduction and the valence band as shown in Fig. 1 for samples of concentrations greater than 5%. For concentrations less than 5%, the overlap energies are calculated from the period of the de Haas-van Alphen effect in pure bismuth and bismuth-antimony alloys.[9]

The behavior of resistivity below 25°K is shown in Fig. 6 and 7 for the whole series of concentrations. In this region the resistivity increases very slowly with decrease in temperature. This change in behavior at 25°K is not at present completely understood in terms of the simple model used to explain the higher temperature behavior. The essential feature of the low temperature behavior is that the resistivity at 4.2°K plotted against concentration (Fig. 9) shows a pronounced maximum at the same concentration at which the maximum activation energy is reached.

In order to assess the nature of the carriers, the two components of Hall effect have been measured for current flowing along the binary axis. We have designated by R_p the values obtained with magnetic field H parallel to the trigonal axis and by R_s those obtained with H perpendicular to both the trigonal and the

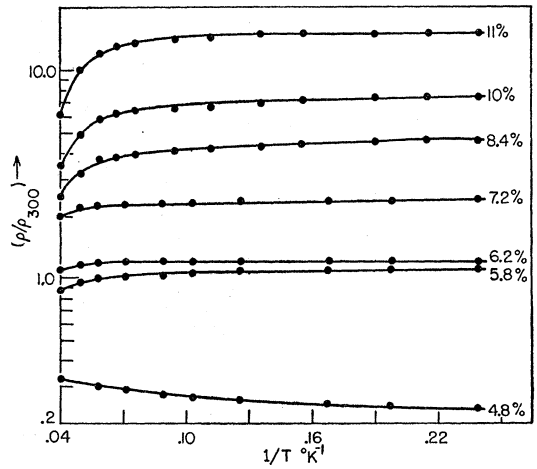

FIG. 6. Low-temperature behavior of the ratio of electrical resistivity to that at 300°K for samples containing 0 to 11% Sb.

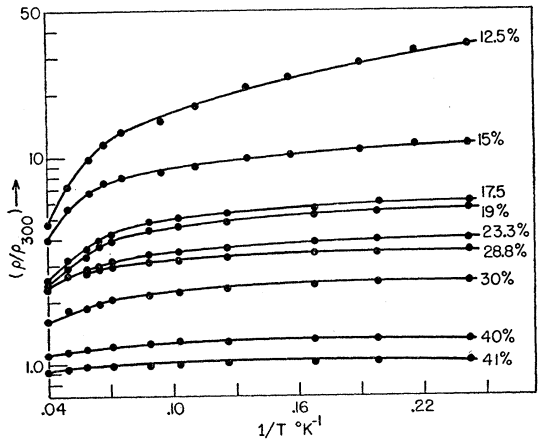

FIG. 7. Low-temperature behavior of the ratio of electrical resistivity to that at 300°K for samples containing 12.5–41% Sb.

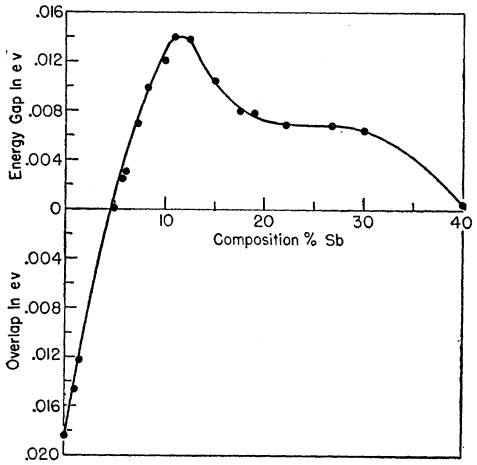

FIG. 8. Activation energy Eg *vs* concentration of Sb.

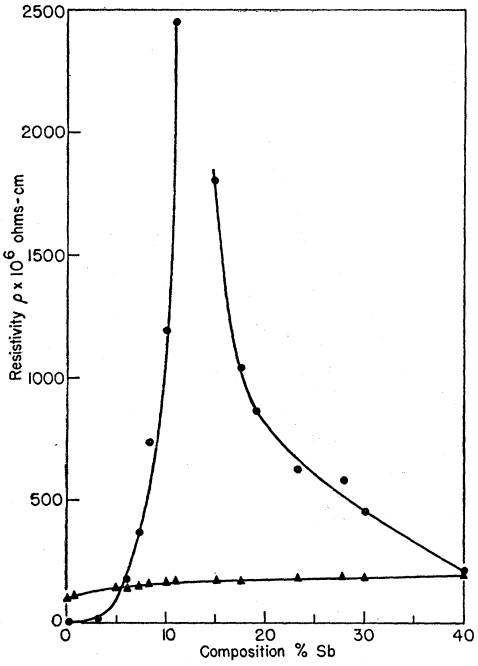

FIG. 9. Resistivity *vs* concentration of Sb. Circles are at 4.2°K and triangles at 300°K.

binary axes of the crystal. For a crystal of rhombohedral symmetry, R_p and R_s are the only two independent components of the Hall coefficient tensor. R_p is always positive above 25°K for the concentration range examined (Figs. 10, 11). Below 25°K, R_p is positive for samples with less than 11.5% Sb but negative above this concentration as is shown in Figs. 10 and 11. On the other hand, R_s is negative for pure bismuth and for samples less than 3% Sb, but Fig. 12 shows R_s to be positive for higher concentrations and remains so over the entire range of temperature. Behavior of R_p and R_s at 4.2°K for different concentrations is as shown in Fig. 13. Magnetoresistance at 4.2°K for current flow along the binary axis and H along the trigonal has also been measured at 1300 oersteds. The results expressed in terms of $\Delta\rho/\rho$ are plotted as a function of concentration in Fig. 14. $\Delta\rho/\rho$ is extremely large for pure bismuth but it tends to decrease on alloying. Below 11.5% Sb concentration, $\Delta\rho/\rho$ shows a complicated behavior. Linear field-dependence for the Hall voltage and quadratic dependence for magnetoresistance was observed for magnetic fields up to about 1400 oersteds, above which they show a more complicated dependence.

Connel and Marcus[15] have observed 6 components of the Hall effect tensor, instead of the two allowed by the 3-fold rotational symmetry, above 3000 oersteds at 77°K and 295°K. However, it appears that this discrepancy is due to a significant contribution coming

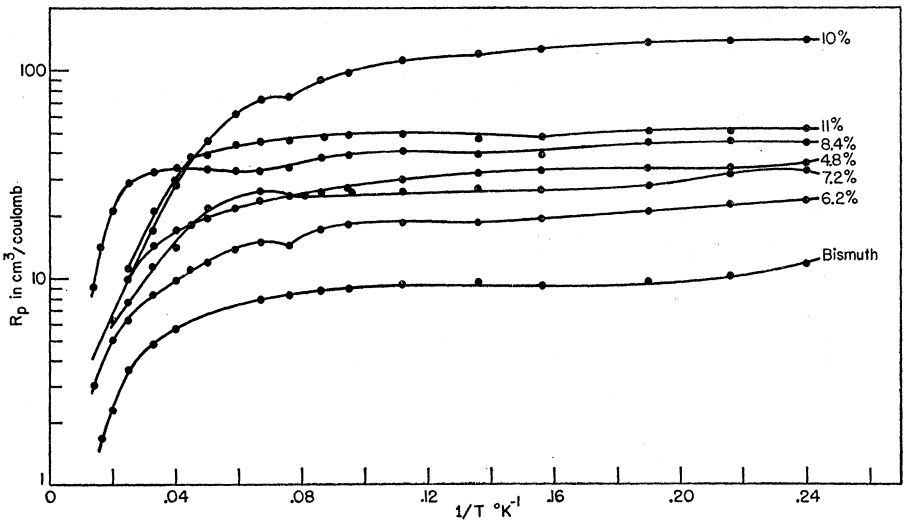

FIG. 10. Hall coefficient R_p *vs* $1/T$. Current along binary axis and H parallel to trigonal axis for 0–11% Sb.

[15] R. A. Connel and J. A. Marcus, Phys. Rev. **107**, 940 (1957).

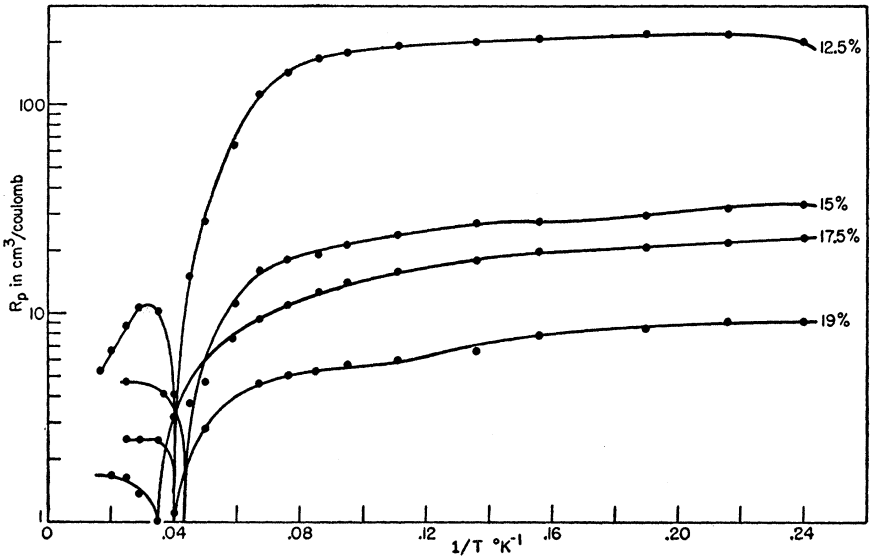

FIG. 11. Hall coefficient R_p *vs* $1/T$ for current along binary axis, H parallel to trigonal axis for 12.5–20% Sb.

from non-linear terms in the magnetic field dependence. When Connel and Marcus's results are extrapolated to low magnetic fields, their results agree with ours to about 20%, i.e., within the uncertainties of the extrapolation.

Lattice Parameter

For simplicity of calculations, the hexagonal lattice was used. The interplanar spacing d_{hkl} for the lattice is given by

$$\frac{1}{d_{hkl}^2}=\frac{4}{3}\frac{h^2+hk+k^2}{a^2}+\left(\frac{l}{c}\right)^2, \qquad (2)$$

where a and c are the lattice parameters. For pure bismuth $a=4.546$ A and $c=11.860$ A at room temperature, the volume of the unit cell being given by $V=236.8\times10^{-24}$ cm³. The parameters c and a for alloys are given as a function of concentration in Fig. 15. Ehret and Abramson[16] and Bowen and Morris-Jones[17] concluded from their measurements that the Vegard's law is obeyed for these alloys. However, their results at low concentrations of antimony were not sufficiently extensive to show the deviations from Vegard's law which have been observed in our work. Some of the values of the lattice parameter c have been recalculated for the hexagonal unit cell from Ehret and Abramson's data and are found to be in agreement with our results within their experimental error of 2 parts per

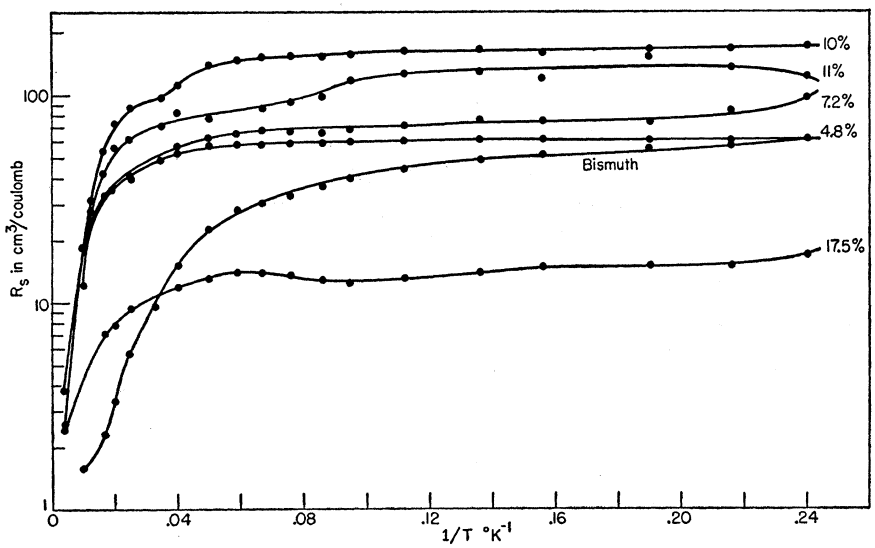

FIG. 12. Hall coefficient R_s *vs* $1/T$ for current along binary axis and H parallel to bisectrix.

[16] W. F. Ehret and M. B. Abramson, J. Am. Chem. Soc. **56**, 385 (1934).
[17] E. G. Bowen and W. Morris-Jones, Phil. Mag. **7**, 1029 (1932).

thousand. The deviations are most marked in the concentration range in which the alloys change from semimetallic to "semiconducting" behavior. The lattice parameters have been determined to an accuracy of one part in a thousand and all the deviations from Vegard's law fall well outside the experimental error.

IV. DISCUSSION

The electrical resistivity and the Hall effect data reported in the previous section for temperatures from 25°K to 300°K can be satisfactorily interpreted in terms of the model proposed by Blount and Cohen. According to this model the essential part of the band structure of pure bismuth [Fig. 1(a)] consists of a pair of light-mass bands at six symmetrically related positions in **k**-space and a heavy-mass hole band at 2 positions in **k**-space. We mark the light mass bands by C_L, V_L and the heavy-mass hole band by V_H as indicated in Fig. 1(a). In pure bismuth, the upper band C_L overlaps slightly upon the heavy-mass hole band so that there is a very small number of light electrons and an equal number of heavy holes.

In order to explain the behavior of alloys in terms of band structure, we assume for the sake of simplicity that the relative positions of C_L and V_L with respect to each other and the curvature of all the three bands remains unaffected on alloying. Then on the addition of antimony, the pair of light mass bands moves up relative to the band V_H, resulting in a decrease of the overlap between C_L and V_H. At a concentration of about 5% Sb, the overlap of C_L and V_H just vanishes and above this concentration an energy gap exists between the light electron band and the heavy hole band. Such a situation is depicted in Fig. 1(b) and probably persists up to about 7.2%. Below 7.2%, the electric conduction is therefore mainly due to the thermal excitation of carriers from the band V_H to C_L. The evidence for such a situation is readily seen from the fact that the extrapolation of the activation energy curve to pure bismuth gives a figure for the overlap energy essentially in agreement with Shoenberg's value. It appears that the band V_L moves up to the same height in the energy *vs* **k** diagram as the band V_H at a concentration of about 7.2%. This figure of 7.2% is obtained by extrapolating the horizontal portion of the activation energy curve to the lower concentration which has the same activation energy as a 20% sample. A justification for this will follow from the discussion given below. Above 7.2% thermal activation should, in principle, take place from both V_H and V_L to C_L. However, because of the high density of states of the band V_H relative to V_L, the activation in the temperature range 30–100°K continues to take place from V_H until it moves considerably farther from V_L. On this scheme, therefore, the maximum activation energy of $Eg \cong 0.014$ ev as determined from high temperature slope at 12% is probably reached when the band edges of two hole bands have moved apart enough to contribute almost equally to the activation process at high temperatures. Beyond 12%, therefore, the effect of the heavy band V_H will be decreasing in comparison with the increasing influence of the light hole band and will correspondingly decrease the apparent activation energy. Since decreasing the temperature from 100°K to 30°K will cause excitation first from C_L to V_H and then from C_L to V_L, a continuous curving of $\log(\rho/\rho_{300})$ *vs* $1/T$ plots from a straight line is observed in this temperature range. On the addition of 18% antimony, the band V_H has probably moved far enough below the pair of bands C_L

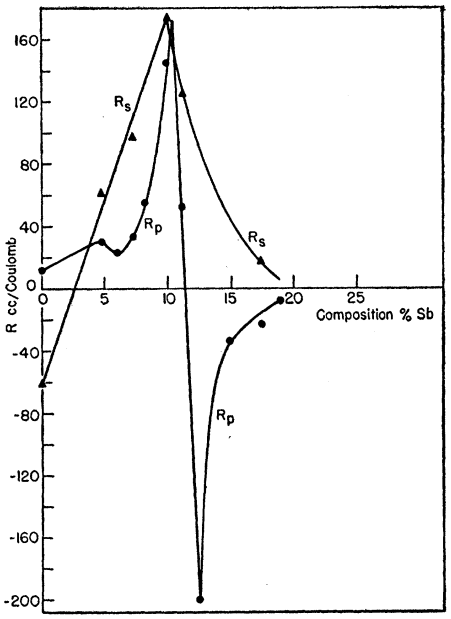

FIG. 13. Behavior of R_p, R_s at 4.2°K as a function of concentration of Sb.

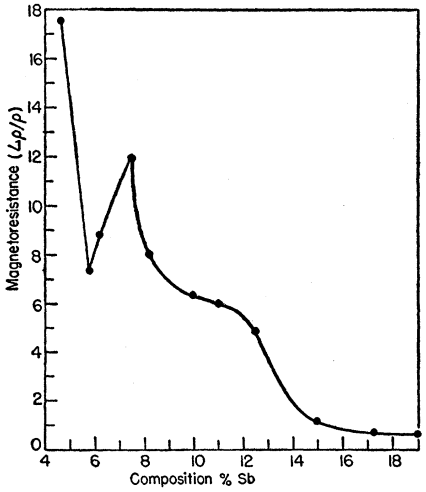

FIG. 14. Magnetoresistance $\Delta\rho/\rho$ at 4.2°K and 1300 Oersteds as a function of concentration of Sb.

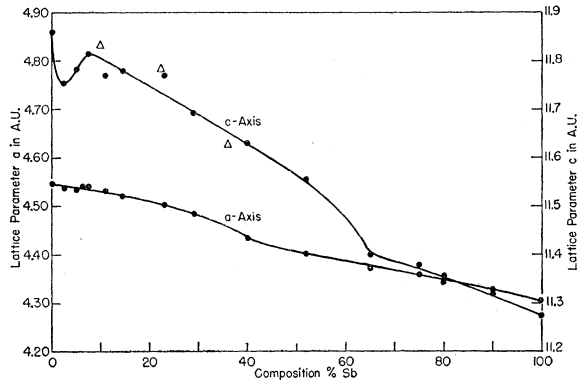

FIG. 15. Lattice parameters C and a plotted against concentration of Sb. Present data indicated by circles; Ehret and Abramson's data shown by triangles.

and V_L for its contribution to be negligible in comparison with that due to V_L. On this model, therefore, the activation energy should remain constant at higher concentrations at a value corresponding to the gap between V_L and C_L. This is observed to be the case up to a concentration of 30%; the corresponding value of the band gap is approximately 0.007 ev. Since beyond 40%, the specimens start showing semimetallic behavior again, it seems likely that the band C_L has started overlapping again on some other set of bands in a manner which will be in accordance with the structure of antimony. Because of the limited knowledge about antimony, it is not possible to infer correctly the nature of bands in alloys beyond 30% concentration.

In order to put the model on a more quantitative basis, it is necessary to calculate the number of carriers for some of the typical situations shown in Fig. 1. However such a calculation requires the knowledge of the mean effective masses of the carriers in all the three bands under consideration. Kalinkina and Strekov have analyzed their specific heat data in terms of 3 ellipsoids for electrons and a single ellipsoid of revolution about the trigonal axis for holes. Using the mean effective mass and the Fermi energy for electrons as deduced from the de Haas-von Alphen effect, they have obtained the corresponding figures for the holes. However, as mentioned earlier, the inversion symmetry of the rhombohedral crystal requires 6 ellipsoids for electrons and in general 2 ellipsoids for holes, thus doubling the total number of carriers. Therefore we have reanalyzed the specific heat data using the mean effective mass of electrons as given by Aubrey and Chambers and the Fermi energy of the electrons as given by Shoenberg. The values of the various parameters for electrons and holes calculated on this model are given in Table III.

Now the total number of electrons/cm³ distributed over all the 6 ellipsoids at any temperature is given by

$$N_e=6\frac{4\pi(2m_e^*)^{\frac{3}{2}}}{h^3}\int_0^\infty\frac{E^{\frac{1}{2}}dE}{e^{(E-\xi_e)/kT}+1}, \tag{3}$$

while the total number of holes/cm³ for two ellipsoids in the valence bands V_h is given by

$$N_h'=2\frac{4\pi(2m_h^*)^{\frac{3}{2}}}{h^3}\int_0^\infty\frac{E^{\frac{1}{2}}dE}{e^{(E-\xi_h')/kT}+1}. \tag{4}$$

Further we may assume that the mean effective mass of holes in band V_L is the same as that of electrons in band C_L because of the very small band gap implied by the small value of the electron mass. The number of holes in band V_L is then given by

$$N_h''=6\frac{4\pi(2m_e^*)^{\frac{3}{2}}}{h^3}\int_0^\infty\frac{E^{\frac{1}{2}}dE}{e^{(E-\xi_h'')/kT}+1}. \tag{5}$$

In these expressions ξ_e, ξ_h', ξ_n'' are the Fermi energies for electrons and holes in bands C_L, V_H, and V_L, respectively. Since there exists only one Fermi level, ξ_e, ξ_h', ξ_h'' are related to each other through the energy gaps between the band edges. Assuming these energy gaps for some typical situations, N_e, N_h', and N_h'' have been calculated as a function of temperature using McDougall and Stoner's tables[18] of Fermi-Dirac functions. The number of carriers at equilibrium has been determined at various temperatures for each of the typical cases graphically by satisfying the following equations for various concentration ranges. For

$$\begin{aligned} &x<7.2\% && N_e=N_h', \\ &x=7.2 \text{ to } 18\%, && N_e=N_h'+N_h'', \\ &x=18 \text{ to } 30\%, && N_e=N_h''. \end{aligned}$$

The results of these calculations are shown in Fig. 16, where the logarithm of the number of carriers has been plotted as a function of $1/T$ for C_L-V_L assumed constant and C_L-V_H varied from -0.0185 ev in pure bismuth to a positive value several times larger than 0.0072 ev so that the effect of V_H becomes negligible.

The results in Fig. 16 can be represented in the temperature range of interest, 30° to 80°K by,

$$N_e\propto T^{\frac{3}{2}}\exp(-E^*/2kT), \tag{6}$$

where E^* is an apparent energy gap. Initially, E^* coincides with C_L-V_H. As C_L-V_H increases further E^* passes through a maximum of roughly 0.02 ev and then decreases to 0.0072 ev, the value assumed for C_L-V_L. The observed dependence of resistivity on temperature

TABLE III. Data relating to fermi surface of bismuth.

	Electrons	Holes
Mean effective mass	$0.039m_0$	$1.5m_0$
Total number of carriers at 4.2°K	4.92×10^{17}/cm³	4.92×10^{17}/cm³
Fermi energy at 4.2°K	0.0177 ev	0.001 ev

[18] J. McDougall and E. C. Stoner, Trans. Roy. Soc. (London) **A237**, 67 (1938).

in this range is consistent with a carrier concentration given by Eq. (6) and with mobilities varying roughly as $T^{-\frac{3}{2}}$, as appears below. It is therefore legitimate to equate the experimentally determined activation energy *vs* concentration in Fig. 8 with E^*. The observed dependence of activation energy, or E^*, *vs* concentration thus appears as a consequence of the monotonic increase of $C_L - V_H$ with concentration predicted by the model.

The concentration dependence of E_g, the energy gap between C_L and V_H at low concentrations, is now given in Fig. 8 according to our model. Using these values of E_g and interpolating between the curves of electron concentration N_e *versus* $1/T$ given in Fig. 16, we can determine the carrier concentrations in the samples studied experimentally. For these samples, an effective mobility $\sigma/N_e e$ can thus be calculated as a function of temperature. For sufficiently low concentrations of Sb, only the light electrons and heavy holes contribute to the mobility so that

$$\sigma/N_e e \cong \bar{\mu}(C_L) + \bar{\mu}(V_H), \tag{7}$$

where the bars signify an appropriate average over the ellipsoids comprising the energy surfaces of the electrons and holes. Figure 17 shows $\log(\sigma/N_e e)$ *vs* $\log T$ between 30°K and 60°K. Assuming a mobility law of the form AT^{-s}, we obtain the values of s given in Table IV. The decrease in s with increasing antimony concentration reflects the increasing role of impurity scattering in the alloys.

The above analyses of the carrier concentrations and the mobilities are by no means complete. In order to determine the complete mobility tensors for the electrons and holes and to establish the carrier concentrations, the correct procedure should be to measure all the components of Hall and magnetoresistance tensors in all alloys as functions of temperature and then analyze the data in terms of the model. With the techniques employed in the present investigation, it was not possible to grow single crystals of alloys having sufficiently different orientations for such a complete analysis. If one assumes that the anisotropies of the mobility tensors in the alloys are the same as for pure bismuth at 4.2°K, then the present resistivity and Hall effect do suffice. This suggested analysis has not yet been carried out for the alloys; nevertheless we report the results for pure bismuth because of their intrinsic interest. Using $N_e = 4.9\times10^{17}/\text{cm}^3$ for bismuth given earlier, the following values of the mobilities for electrons and holes have been obtained from the best fit of the experimental data to the expressions given by Abeles and Meiboom[3]:

$$\mu_1 = 14.1\times10^6 \text{ cm}^2/\text{volts-sec},$$
$$\mu_2 = 1.5\times10^6 \text{ cm}^2/\text{volts-sec},$$
$$6_3 = 8.3\times10^6 \text{ cm}^2/\text{volts-sec},$$
$$\nu_1 = \nu_2 = 4.8\times10^6 \text{ cm}^2/\text{volt-sec},$$
$$\nu_3 = 4.4\times10^6 \text{ cm}^2/\text{volt-sec},$$

where μ's are for electrons and ν's for holes. The subscripts 1, 2, 3 refer to the binary, bisectrix, and trigonal axes, respectively. These estimates show that the electron and hole mobilities are comparable in magnitude but that the electron mobility tensor is anisotropic

TABLE IV. Effective mobility at 40°K as function of Sb concentration.

Concentration	$N_e\times10^{-17}(\text{cm}^{-3})$	$\sigma/N_e e\left(\frac{\text{cm}^2}{\text{volt-sec}}\right)$	s
0%	7.6	0.49×10^6	1.7
4.8%	2.3	0.44×10^6	1.8
5.8%	1.9	0.29×10^6	1.4
7.2%	1.2	0.24×10^6	1.4

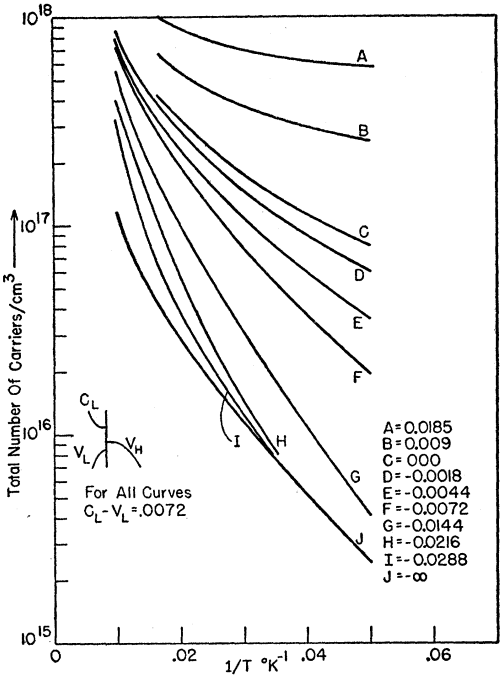

FIG. 16. Logarithm of the number of carriers *vs* $1/T$ between 20°K to 100°K.

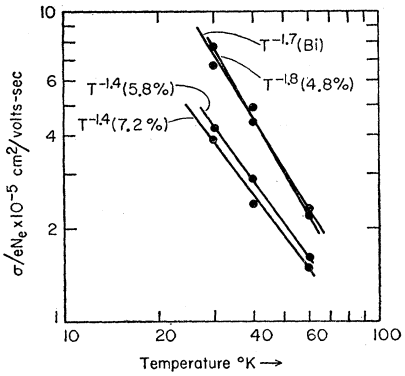

FIG. 17. $\log(\sigma/N_e e)$ *vs* $\log T$ between 30°K and 60°K for samples containing 0–7.2% Sb.

whereas the hole mobility tensor is not. The anisotropy of the electron mobility tensor, however, is much less than what would be expected from the anisotropy of the effective mass tensor on the approximation of isotropic relaxation time, but about what would be expected on the approximation of isotropic mean free path.

For temperatures below 25°K, both resistivity and Hall coefficients show a weak dependence on temperature. This behavior is not easily explicable in terms of Blount and Cohen's model, which would lead to a continued exponential temperature dependence below 25°K. The data suggests another overlap between the conduction and valence bands. However, the dependence of this overlap on concentration would appear to be rather complicated. An alternative source of the low-temperature behavior may possibly be the fuzzing of the band edges C_L, V_L, and V_H on alloying. At this stage it is not possible to decide which, if either, of the two alternatives is correct.

To summarize, the behavior of the resistivity as a function of antimony concentration above 25°K can be explained semiquantitatively in terms of the model proposed by Blount and Cohen. In particular, behavior resembling the semiconductivity predicted by Heine is observed. However, the behavior below 25°K shows that the model is incomplete and additional complications may occur in the band structure of the alloys and possibly also of pure bismuth.

ACKNOWLEDGMENTS

The author wishes to express his gratitude to his sponsor, Professor A. W. Lawson, for advice and encouragement, to Professor M. H. Cohen for enlightening conversations concerning the theoretical interpretation of the data, and to Dr. M. Bachelder for the chemical analysis of the alloys. He is also indebted to the U. S. Educational Foundation in India for the award of a Fulbright Scholarship and to the University of Chicago for a Graduate Fellowship.

PHYSICAL REVIEW VOLUME 114, NUMBER 6 JUNE 15, 1959

Hartree-Fock Theory with Nonorthogonal Basis Functions

R. McWEENY
Departments of Mathematics, Physics, and Chemistry, University College of North Staffordshire, Keele, Staffordshire, England
(Received January 19, 1959)

Solutions of the Hartree-Fock self-consistent-field equations can be approximated by linear combination of a set of basis functions: the equations then assume a matrix form, as shown by Roothaan. It is possible, however, to obtain the required variational solution of the many-electron problem much more directly by an iterative construction of the density matrix. This method, first developed by the author for expansion in terms of orthogonal basis functions, is extended to the case of a nonorthogonal set.

INTRODUCTION

DURING recent years two modifications of the Hartree-Fock self-consistent-field (SCF) theory have been developed. Numerical integration can be avoided by determining the occupied orbitals as linear combinations of an arbitrary (in principle complete) set of basis functions[1] and the repeated solution of an eigenvalue problem can be avoided by means of a density matrix formulation, followed by direct iterative construction of the density matrix.[2] This note is concerned with the extension of the iterative process to the case in which the basis functions are nonorthogonal.

Let us represent the n doubly occupied SCF orbitals $(A,B,C,\cdots)$ in terms of m nonorthogonal basis functions $(a,b,c,\cdots)$, with overlap matrix S, by

$$(A\ B\ C\cdots)=(a\ b\ c\cdots)\mathbf{T}, \tag{1}$$

where $\mathbf{T}$ is an $m\times n$ matrix. The density matrices (and hence the energy and the expectation values of all other dynamical quantities) are then determined by the invariant $\mathbf{R}=\mathbf{T}\mathbf{T}^\dagger$. The (spinless) one-particle density matrix is $\mathbf{P}=2\mathbf{R}$ and if we assume a Hamiltonian

$$H=\sum_i f(i)+\tfrac{1}{2}\sum_{i,j}{}' g(i,j),$$

the energy is given by[2]

$$E=2\ \mathrm{tr}\ \mathbf{R}\mathbf{f}+\mathrm{tr}\ \mathbf{R}\mathbf{G}, \tag{2}$$

where, with a standard notation, the matrix elements are

$$\begin{aligned} f_{ab}&=(a|f|b),\\ G_{ab}&=\textstyle\sum_{rs} R_{rs}[2(as|g|br)-(as|g|rb)]. \end{aligned} \tag{3}$$

The electron interaction matrix is $\mathbf{R}$ dependent, $\mathbf{G}=\mathbf{G}(\mathbf{R})$, and leads to a nonlinear problem. According to the variation theorem, the best approximate SCF function results when E of (2) is minimized subject to preservation of orthonormality of the occupied orbitals $A,B,\cdots$. In the case of orthornormal *basis* functions, $\mathbf{S}=\mathbf{1}_m$, and the constraint is simply $\mathbf{T}^\dagger\mathbf{T}=\mathbf{1}_n$. An

[1] C. C. J. Roothaan, Revs. Modern Phys. **23**, 61 (1957).
[2] R. McWeeny, Proc. Roy. Soc. (London) **A235**, 496 (1956).